

# Time-dependent density functional theory for a unified description of ultrafast dynamics: pulsed light, electrons, and atoms in crystalline solids

Atsushi Yamada\* and Kazuhiro Yabana  
 Center for Computational Sciences, University of Tsukuba,  
 1-1-1 Tennodai, Tsukuba, Ibaraki 305-8577, Japan  
 (Dated: October 16, 2018)

We have developed a novel multiscale computational scheme to describe coupled dynamics of light electromagnetic field with electrons and atoms in crystalline solids, where first-principles molecular dynamics based on time-dependent density functional theory is used to describe the microscopic dynamics. The method is applicable to wide phenomena in nonlinear and ultrafast optics. To show usefulness of the method, we apply it to a pump-probe measurement of coherent phonon in diamond where a Raman amplification takes place during the propagation of the probe pulse.

Nonlinear optics in solids is the study of the interaction of intense laser light with bulk materials [1–3]. It is intrinsically a complex phenomena arising from a coupled nonlinear dynamics of light electromagnetic fields, electrons, and phonons. They are characterized by two different spatial scales, micro-meter for the wavelength of the light and less than nano-meter for the dynamics of electrons and atoms.

In early development, nonlinear optics has developed mainly in perturbative regime and in frequency domain[4, 5]. However, it has changed rapidly and drastically. Nowadays, measurements are carried out quite often in time domain using pump-probe technique as a typical method and the time resolution reaches a few tens of attosecond[6, 7]. Extremely nonlinear phenomena has attracted interests such as high harmonic generation in solids[8, 9], ultrafast control of electrons motion in dielectrics that aims for future signal processing using pulsed light[10–12], and ultrafast coherent optical phonon control[13–22] and photoinduced structural phase transition of materials[23–26].

In this paper, we report a progress to develop first-principles computational method to describe nonlinear optical processes in solids that arise from coupled dynamics of light electromagnetic fields, electrons, and atoms in crystalline solids. In condensed matter physics and materials sciences, first-principles computational approaches represented by density functional theory have been widely used and recognized as an indispensable tool[27]. Development of first-principles approaches in optical sciences is, however, still in premature stage due to the complexity of the phenomena and the requirement of describing time-dependent dynamics.

Our method utilize time-dependent density functional theory (TDDFT) for microscopic dynamics of electrons[28, 29]. The TDDFT is an extension of the density functional theory so as to be applicable to electron dynamics in real time[30]. In microscopic scale, ultrafast dynamics of electrons have been successfully explored solving the time-dependent Kohn-Sham (TDKS) equation, the basic equation of TDDFT, in real time[31–33]. We have further developed a multiscale scheme coupling

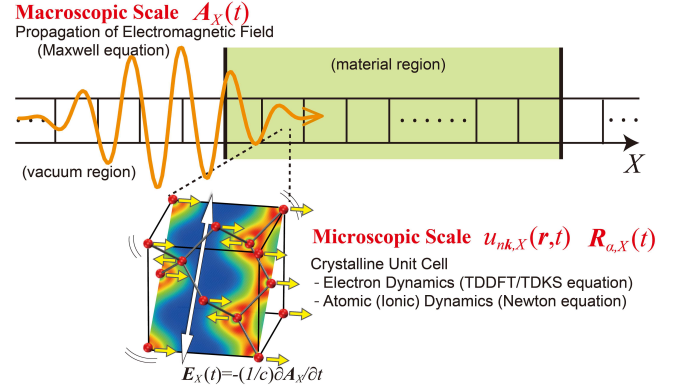


FIG. 1. Schematic illustration of the multiscale scheme for a light propagation through a material.

the light electromagnetic fields and electrons in solids[34], and applied it to investigate extremely nonlinear optical processes in dielectrics using few-cycle femtosecond pulses[11, 12]. Here we extend the approach to incorporate atomic motion, combining first-principles molecular dynamics approach[35]. It will then be capable of describing vast nonlinear optical phenomena involving atomic motion such as stimulated Raman scattering[1–3] that will be discussed later in this paper.

We consider a problem of an ultrashort pulsed light irradiation normally on a thin dielectric film, as illustrated in Fig.1. In our multiscale description [34], we introduce two coordinate systems, the macroscopic coordinate  $X$  that is used to describe the propagation of the light electromagnetic fields, and the microscopic coordinates  $\mathbf{r}$  for the dynamics of electrons and atoms.

The light electromagnetic field is expressed by using a vector potential  $\mathbf{A}_X(t)$  that satisfies the Maxwell equation,

$$\left[ \frac{1}{c^2} \frac{\partial^2}{\partial t^2} - \frac{\partial^2}{\partial X^2} \right] \mathbf{A}_X(t) = \frac{4\pi}{c} \mathbf{J}_X(t), \quad (1)$$

where  $\mathbf{J}_X(t)$  is the electric current density at the point  $X$ .

We will use a uniform grid for the coordinate  $X$  to solve Eq.(1). At each grid point  $X$ , we consider an

infinitely periodic medium composed of electrons and atoms whose motion are described using the microscopic coordinate  $\mathbf{r}$ . Since the wavelength of the pulsed light is much longer than the typical spatial scale of the microscopic dynamics of electrons and atoms, we assume a dipole approximation: At each point  $X$ , the electrons and atoms evolve under a spatially-uniform electric field,  $E_X(t) = -(1/c)(\partial A_X(t)/\partial t)$ . Then we may apply the Bloch theorem at each time  $t$  in the unit cell, and may describe the electron motion using Bloch orbitals  $u_{n\mathbf{k},X}(\mathbf{r}, t)$  with the band index  $n$  and the crystalline momentum  $\mathbf{k}$  [36]. Atomic motion can also be described by atomic coordinates in the unit cell,  $\mathbf{R}_{\alpha,X}(t)$ , where the index  $\alpha$  distinguishes different atoms in the unit cell.

The Bloch orbitals satisfy the TDKS equation,

$$i\hbar \frac{\partial}{\partial t} u_{n\mathbf{k},X}(\mathbf{r}, t) = \left[ \frac{1}{2m} \left\{ -i\hbar \nabla_{\mathbf{r}} + \hbar \mathbf{k} + \frac{e}{c} \mathbf{A}_X(t) \right\}^2 - e\phi_X(\mathbf{r}, t) + \frac{\delta E_{XC}[n_{e,X}]}{\delta n_{e,X}} + \hat{v}_{ion,X}(\mathbf{r}; \{\mathbf{R}_{\alpha,X}(t)\}) \right] u_{n\mathbf{k},X}(\mathbf{r}, t) \quad (2)$$

where  $n_{e,X}$  is the electron density given by  $n_{e,X}(\mathbf{r}, t) = \sum_{n,\mathbf{k}} |u_{n\mathbf{k},X}(\mathbf{r}, t)|^2$ .  $\phi_X(\mathbf{r}, t)$  and  $E_{XC}[n_{e,X}]$  are the Hartree potential and the exchange-correlation energy, respectively.  $\hat{v}_{ion,X}(\mathbf{r}; \{\mathbf{R}_{\alpha,X}(t)\})$  is the electron-ion potential for which we use norm-conserving pseudopotential [37].

To describe the dynamics of atoms, we use a so-called Ehrenfest dynamics [28] where the atomic motion is described with mean-field from the electrons by the Newton equation,

$$M_{\alpha} \frac{d^2 \mathbf{R}_{\alpha,X}}{dt^2} = -\frac{eZ_{\alpha}}{c} \frac{d\mathbf{A}_X}{dt} + \frac{\partial}{\partial \mathbf{R}_{\alpha,X}} \int d\mathbf{r} [en_{ion,X} \phi_X(\mathbf{r})] \quad (3)$$

where  $M_{\alpha}$  is the mass of the  $\alpha$ -th ion,  $n_{ion,X}$  is the charge density of ions given by  $n_{ion,X}(\mathbf{r}, \{\mathbf{R}_{\alpha,X}(t)\}) = \sum_{\alpha} Z_{\alpha} \delta(\mathbf{r} - \mathbf{R}_{\alpha,X}(t))$ , with  $Z_{\alpha}$  the charge number of the  $\alpha$ -th ion.

The electric current density at point  $X$ ,  $\mathbf{J}_X(t)$ , consists of electronic and ionic contributions,

$$\mathbf{J}_X(t) = \mathbf{J}_{e,X}(t) + \mathbf{J}_{ion,X}(t). \quad (4)$$

The electronic component  $\mathbf{J}_{e,X}(t)$  is given by the Bloch orbitals  $u_{n\mathbf{k},X}(\mathbf{r}, t)$  [34]. The ionic component is given by  $\mathbf{J}_{ion,X}(t) = e \sum_{\alpha} Z_{\alpha} (d\mathbf{R}_{\alpha,X}(t)/dt)/\Omega$ , where  $\Omega$  is the volume of the unit cell.

We solve Eqs. (1) - (4) simultaneously to obtain the whole dynamics at once with the initial condition that the electronic state at each point  $X$  is set to the ground state solution of the static density functional theory, atomic positions are set to their equilibrium position in the electronic ground state, and the vector potential of the incident pulsed light is set in the vacuum region in front of the thin film. We note that the present scheme naturally

includes the ordinary macroscopic electromagnetism in a weak field limit, since solving the TDKS equation (2) is equivalent to utilizing the linear constitutive relation for a weak field.

Now, we apply the method to describe the pump-probe measurement that aims to investigate the generation of coherent optical phonons [19]. We consider a diamond thin film of 6  $\mu\text{m}$  thickness, and two linearly-polarized pulses are irradiated successively and normally on the surface. We set the crystalline  $abc$  axes of cubic diamond to coincide with the  $xyz$  axes of the Cartesian coordinates, respectively.

We implemented our scheme in the open-source software SALMON [38, 39] which utilizes real-space uniform grid representation to express orbitals. Since a number of microscopic dynamics are calculated simultaneously in the multiscale scheme, we use a massively parallel super-computer with an efficient implementation of parallelization [40]. Adiabatic local density approximation is used for the exchange-correlation potential [41]. The  $X$  coordinate from  $X=0$  to 6  $\mu\text{m}$  is discretized by 400 grid points with the spacing of 15 nm. The microscopic unit cell of diamond consists of eight carbon atoms in the cubic cell of the side length of 3.567 Å. The Bloch orbitals are expressed using  $16^3$  uniform spatial grids in the unit cell and  $12^3$  of  $k$ -points in the Brillouin zone. The time step is chosen as 2 as.

We first show the calculation for the generation of the coherent phonon by the pump pulse. Figure 2(a) shows the propagation of the pump light and the displacement of the atoms at different macroscopic point  $X$ . The frequencies and the pulse duration of the pump pulse is set to 1.55 eV/ $\hbar$  and 6.5 fs in FWHM, respectively. The pulse duration is chosen to be shorter than the period of the optical phonon of diamond, 25 fs. The polarization direction of the pump pulse is chosen as [011] direction, which causes the optical phonon in [100] direction. The maximum intensity of the pump pulse is set to  $2 \times 10^{12}$  W/cm<sup>2</sup>.

When the pump field propagates through the material, the harmonic motion of atoms is generated in turn at each  $X$  position. In Fig. 2(a), a wave-like behavior of atomic displacement is seen along the  $X$  axis. However, this is not an ordinary phonon wave described by the lattice dynamics. The period of the oscillation at each  $X$  position is the period of the optical phonon which is 25 fs, and the speed of the propagation is equal to the speed of the pump pulse in the medium,  $c/n$ , with the index of refraction  $n$ .

In Fig.2(b), the generation process of the optical phonon at  $X=2 \mu\text{m}$  is shown as a function of time. At first, the force is proportional to the square of the electric field. As the phonon starts to move, the restoring force begins to work. These behavior of the force and the generation process of the coherent phonon is consistent with the picture of the impulsively stimulated Raman scatter-

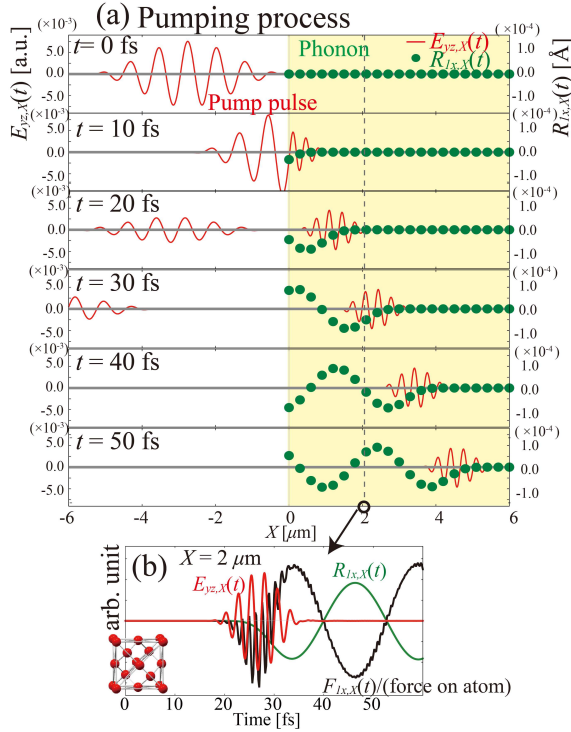


FIG. 2. (a) Snapshots of the electric field of the pump pulse (red lines) and the atomic displacement (green filled circles) are shown along the macroscopic position  $X$ . (b) Electric field of the pump pulse (red line), the force acting on the atom (black line), and the atomic displacement (green line) are shown at  $X = 2 \mu\text{m}$  as a function of time.

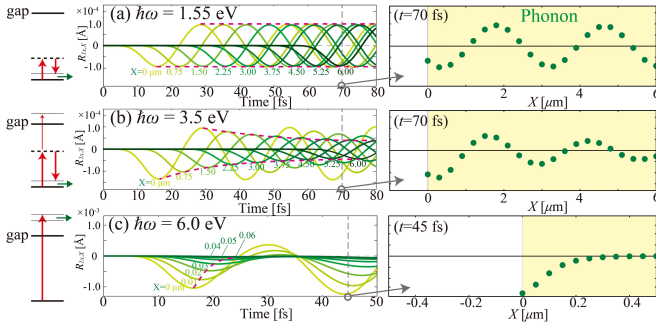


FIG. 3. Coherent phonon generation by pump pulses of three different frequencies,  $\hbar\omega =$  (a) 1.55, (b) 3.5 and (c) 6.0 eV. The atomic displacements as a function of time are shown at selected macroscopic positions of  $X$  (the left panels) and those along the coordinate  $X$  at specific times (the right panels).

ing (ISRS) mechanism[19]. After the pump field passes away, there is no driving force and a simple harmonic motion of atoms continues without decay.

We next show in Fig.3 the generation of coherent phonons by pulses of three different frequencies. Panel (a) shows the generation with  $\hbar\omega = 1.55$  eV, the same as that shown in Fig.2(a). Here the ISRS mechanism is responsible for the coherent phonon generation as mentioned above, since the frequency is below the optical

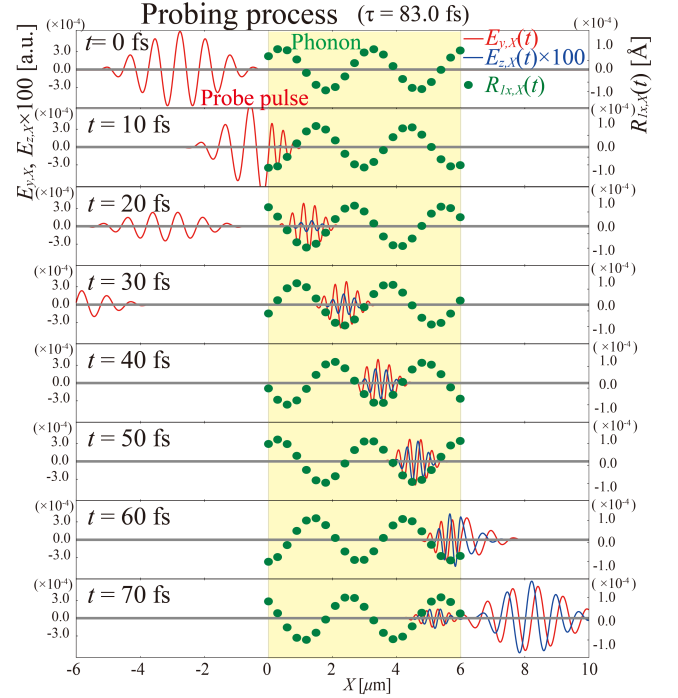


FIG. 4. Snapshots of the electric field of the probe pulse in [010] (red-line) and in [001] (blue-line) polarization directions, and the atomic displacement (green filled circles) are shown along the macroscopic coordinate  $X$ .

gap energy. At  $\hbar\omega = 3.5$  eV, the pump frequency is still below the optical gap energy. However, Fig.3(b) shows that the phonon amplitude decays with  $X$  whereas the amplitude at each position  $X$  does not decay with time. This is caused by the two photon absorption of the pump pulse. Since the pump pulse is rather strong with the intensity,  $2 \times 10^{12}$  W/cm<sup>2</sup>, the pump pulse excites electrons and loses energy as it propagate through the medium.

At  $\hbar\omega = 6$  eV that is above the optical gap energy, the generated phonon amplitude at the solid surface is one order of magnitude larger than the non-resonant cases, as seen in Fig.3(c), The displacement of atoms shows a harmonic motion of cosine shape, namely the oscillation takes place around the shifted equilibrium position. This is due to the change of the generation mechanism from ISRS to the displacive excitation of coherent phonon (DECP) [19]. The amplitude of the phonon decays with  $X$  as the field gets weaker by the absorption of the pulse. These results are consistent with Ref. [33] where generation mechanisms of coherent phonons are discussed without describing the light propagation.

We next proceed to the calculation of the propagation of probe pulses. Although it is possible to carry out the pump and the probe pulse propagations in a single calculation, we separate them since the reflection of the pump pulse at the back surface of the thin film complicates the analyses. In the probe pulse calculation, we prepare the initial medium in which the coherent phonon already ex-

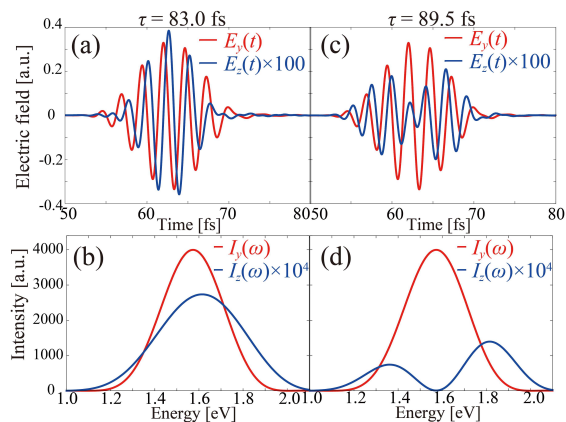


FIG. 5. (a) Transmission wave in the right vacuum region and (b) the Fourier transformed power spectrum with  $\tau = 83.0$  fs. Those with  $\tau = 89.5$  fs are shown in (c) and (d).

ists and irradiate the probe pulse from the vacuum. The phonon motion is in [100] direction as discussed above, and we choose the polarization direction of the probe pulse as [010]. Then we expect the emergence and the amplification of the stimulated Raman wave polarized along [001] direction due to the structure of the Raman tensor of the diamond [42]. The intensity of the probe pulse is set sufficiently small,  $10^{10}$  W/cm<sup>2</sup>, so that there occurs no significant nonlinearity related to the probe pulse.

We show the propagation of the probe pulse and the amplification process of the stimulated Raman wave in Fig.4. In the figure, the probe pulse is irradiated with the pump-probe delay time of  $\tau = 83.0$  fs. At this time delay, the center of the probe pulse moves with the maximum of the phonon amplitude, as seen from the figure. Since, as we noted above, the phonon "wave" propagates with the speed of the pump pulse in the medium and the speeds of the pump and the probe pulses are the same, the probe pulse always stay at the maximum of the phonon. During the propagation of the probe pulse in the medium, we find that the wave polarized along [001] direction generated by the stimulated Raman scattering is amplified linearly in amplitude with the traveled distance with the phase shift of  $\pi/2$  relative to the probe pulse. These features are consistent with a description in standard theoretical description for the stimulated Raman scattering [19, 43].

Finally, we compare in Fig.5 the pulse shape of the probe pulse after it passes out through the thin film for two different pump-probe time differences: Panel (a) is the case of  $\tau = 83.0$  fs, the same as that shown in Fig. 4. Panel (b) is the case of  $\tau = 89.5$  fs, at which the probe pulse moves with the nodal point of the phonon.

In the case of  $\tau = 83.0$  fs, the pulse shape of the stimulated Raman wave is similar to the shape of the probe pulse, with the phase difference of  $\pi/2$ . On the other hand, in the case of  $\tau = 89.5$  fs, the pulse shape of the stimulated Raman wave is very different from the shape

of the probe pulse. This difference can be understood as being originated from the difference of the electric current density that produces the stimulated Raman wave. The electric current density that produce the Raman wave is given by  $J_{\text{Raman}}(t) \propto Q(t)E_{\text{probe}}(t)$  [19, 43], where  $E_{\text{probe}}(t)$  is the electric field of the probe pulse and  $Q(t)$  is the phonon amplitude given by the linear combination of  $\{\mathbf{R}_\alpha(t)\}$ . When the probe pulse enters the medium at the maximum of the phonon amplitude,  $Q(t)$  may be roughly regarded as a constant and  $J_{\text{Raman}}(t)$  is mostly proportional to  $E_{\text{probe}}(t)$  since the half period of the phonon is longer than the duration of the probe pulse. However, when the probe pulse moves with the nodal position of the phonon, the phonon amplitude is approximated by a linear function of time changing the sign. Then, we have  $J_{\text{Raman}}(t) \propto tE_{\text{probe}}(t)$ , and the phonon motion produces one extra node to the electric current density. This explains the shape change of the stimulated Raman wave shown in Fig.5(b).

We show the power spectra of the stimulated Raman waves in panels (b) and (d). Reflecting the difference in the time profile, the power spectra also show a distinct structures: the double-peak structure appears in the power spectrum of the stimulated Raman wave traveling with the nodal point of phonon. We note that such double-peak structure is indeed related to recent pump-probe measurement of the coherent phonon in diamond and other insulators [14, 17]. We will report our analysis for this problem in a separate publication.

In summary, we have developed a computational approach for nonlinear light-matter interaction in solids based on first-principles time-dependent density functional theory. A multiscale scheme is developed simultaneously solving Maxwell equations for light propagation, time-dependent Kohn-Sham equation for electrons, and Newton equation for atoms. As a test example, a pump-probe measurement of coherent phonon generation in diamond is simulated where an amplification by the stimulated Raman scattering is observed for the probe pulse. We expect the method will be useful for a wide phenomena of nonlinear and ultrafast optics.

We acknowledge the supports by JST-CREST under grant number JP-MJCR16N5, and by MEXT as a priority issue theme 7 to be tackled by using Post-K Computer, and by JSPS KAKENHI Grant Number 15H03674. Calculations are carried out at Oakforest-PACS at JCAHPC through the Multidisciplinary Cooperative Research Program in CCS, University of Tsukuba, and through the HPCI System Research Project (Project ID: hp180088).

\* ayamada@ccs.tsukuba.ac.jp

[1] Robert W. Boyd. *Nonlinear Optics, Third Edition*. Aca-

- demic Press, Inc., Orlando, FL, USA, 3rd edition, 2008.
- [2] Y. R. Shen. *The Principles of Nonlinear Optics*. Wiley-Interscience, 1st edition, 1984.
  - [3] Nicolaas Bloembergen. *Nonlinear Optics*. World Scientific, 4th edition, 1996.
  - [4] Joseph W. Goodman. *Introduction to Fourier optics*. Roberts & Company Publishers, Englewood, Colorado, USA, 3rd edition, 2005.
  - [5] Eugene Hecht. *OPTICS*. Pearson Education, Inc., San Francisco, CA, USA, 4ed edition, 2002.
  - [6] Ferenc Krausz and Misha Ivanov. Attosecond physics. *Rev. Mod. Phys.*, 81:163–234, Feb 2009.
  - [7] Francesca Calegari, Giuseppe Sansone, Salvatore Stagira, Caterina Vozzi, and Mauro Nisoli. Advances in attosecond science. *J. Phys. B: At. Mol. Opt. Phys.*, 49:062001, 2016.
  - [8] Shambhu Ghimire, Anthony D. DiChiara, Emily Sistrunk, Pierre Agostini, Louis F. DiMauro, and David A. Reis. Observation of high-order harmonic generation in a bulk crystal. *Nature Physics*, 7:138 EP –, 12 2010.
  - [9] T. T. Luu, M. Garg, S. Yu. Kruchinin, A. Moulet, M. Th. Hassan, and E. Goulielmakis. Extreme ultraviolet high-harmonic spectroscopy of solids. *Nature*, 521:498 EP –, 05 2015.
  - [10] Martin Schultze, Krupa Ramasesha, C. D. Pemmaraju, S. A. Sato, D. Whitmore, A. Gandman, James S. Prell, L. J. Borja, D. Prendergast, K. Yabana, Daniel M. Neumark, and Stephen R. Leone. Attosecond band-gap dynamics in silicon. *SCIENCE*, 346(6215):1348–1352, DEC 12 2014.
  - [11] A. Sommer, E. M. Bothschafter, S. A. Sato, C. Jakubeit, T. Latka, O. Razskazovskaya, H. Fattahi, M. Jobst, W. Schweinberger, V. Shirvanyan, V. S. Yakovlev, R. Kienberger, K. Yabana, N. Karpowicz, M. Schultze, and F. Krausz. Attosecond nonlinear polarization and light-matter energy transfer in solids. *NATURE*, 534(7605):86–90, JUN 2 2016.
  - [12] M. Lucchini, S. A. Sato, A. Ludwig, J. Herrmann, M. Volkov, L. Kasmir, Y. Shinohara, K. Yabana, L. Gallmann, and U. Keller. Attosecond dynamical Franz-Keldysh effect in polycrystalline diamond. *SCIENCE*, 353(6302):916–919, AUG 26 2016.
  - [13] Muneaki Hase, Masahiro Kitajima, Anca Monia Constantinescu, and Hrvoje Petek. The birth of a quasiparticle in silicon observed in time-frequency space. *Nature*, 426:51–54, 2003.
  - [14] K. Mizoguchi, R. Morishita, and G. Oohata. Generation of coherent phonons in a cdtc single crystal using an ultrafast two-phonon laser-excitation process. *Phys. Rev. Lett.*, 110:077402, Feb 2013.
  - [15] I. Katayama, K. Sato, S. Koga, J. Takeda, S. Hishita, H. Fukidome, M. Suemitsu, and M. Kitajima. Coherent nanoscale optical-phonon wave packet in graphene layers. *Phys. Rev. B*, 88:245406, 2013.
  - [16] K. Sato, K. Tahara, Y. Minami, I. Katayama, M. Kitajima, H. Kawai, K. Yanagi, and J. Takeda. Resonance enhancement of first- and second-order coherent phonons in metallic single-walled carbon nanotubes. *Phys. Rev. B*, 90:235435, 2014.
  - [17] Kazutaka G. Nakamura, Kazuma Ohya, Hiroshi Takahashi, Tetsuya Tsuruta, Hiroya Sasaki, Shin-ichi Uozumi, Katsura Norimatsu, Masahiro Kitajima, Yutaka Shikano, and Yosuke Kayanuma. Spectrally resolved detection in transient-reflectivity measurements of coherent optical phonons in diamond. *Phys. Rev. B*, 94:024303, Jul 2016.
  - [18] Hiroya Sasaki, Riho Tanaka, Yasuaki Okano, Fujio Minami, Yosuke Kayanuma, Yutaka Shikano, and Kazutaka G. Nakamura. Coherent control theory and experiment of optical phonons in diamond. *Scientific Reports*, 8:9609, 2018.
  - [19] R. Merlin. Generating coherent thz phonons with light pulses. *Solid State Communications*, 102(2):207 – 220, 1997. Highlights in Condensed Matter Physics and Materials Science.
  - [20] T. E. Stevens, J. Kuhl, and R. Merlin. Coherent phonon generation and the two stimulated raman tensors. *Phys. Rev. B*, 65:144304, 2002.
  - [21] C. Thomsen, J. Strait, Z. Vardeny, H. J. Maris, J. Tauc, and J. J. Hauser. Coherent phonon generation and detection by picosecond light pulses. *Phys. Rev. Lett.*, 53:989, 1984.
  - [22] G. C. Cho, W. Kütt, and H. Kurz. Subpicosecond time-resolved coherent-phonon oscillations in gaas. *Phys. Rev. Lett.*, 65:764, 1990.
  - [23] K. Iwano, Y. Shimoi, T. Miyamoto, D. Hata, M. Sotome, N. Kida, S. Horiuchi, and H. Okamoto. Ultrafast photoinduced electric-polarization switching in a hydrogen-bonded ferroelectric crystal. *Phys. Rev. Lett.*, 118:107404, 2017.
  - [24] Sachio Horiuchi, Kensuke Kobayashi, Reiji Kumai, and Shoji Ishibashi. Proton tautomerism for strong polarization switching. *Nature Communications*, 8(14426), 2017.
  - [25] T. Frigge, B. Hafke, T. Witte, B. Krenzer, C. Streubühr, A. Samad Syed, V. Mikšić Trontl, I. Avigo, P. Zhou, M. Ligges, D. von der Linde, U. Bovensiepen, M. Horn von Hoegen, S. Wippermann, A. Lücke, S. Sanna, U. Gerstmann, and W. G. Schmidt. Optically excited structural transition in atomic wires on surfaces at the quantum limit. *Nature*, 544:207, 2017.
  - [26] Marieke F. Jagera, Christian Otta, Peter M. Krausa, Christopher J. Kaplana, Winston Pousea, Robert E. Marvelc, Richard F. Haglundc, Daniel M. Neumarka, and Stephen R. Leone. Tracking the insulator-to-metal phase transition in vo<sub>2</sub> with few-femtosecond extreme uv transient absorption spectroscopy. *PNAS*, 114:9558–9563, 2017.
  - [27] Richard M. Martin. *Electronic Structure: Basic Theory and Practical Methods*. Cambridge University Press, 2004.
  - [28] Carsten A. Ullrich. *Time-Dependent Density-Functional Theory: Concepts and Applications (Oxford Graduate Texts)*. Oxford Univ Pr (Txt), 2 2012.
  - [29] Miguel A.L. Marques, Neepa T. Maitra, Fernando M.S. Nogueira, E.K.U. Gross, and Angel Rubio, editors. *Fundamentals of Time-Dependent Density Functional Theory (Lecture Notes in Physics)*. Springer, 2012 edition, 1 2012.
  - [30] Erich Runge and Eberhard KU Gross. Density-functional theory for time-dependent systems. *Physical Review Letters*, 52(12):997, 1984.
  - [31] K. Yabana and G. F. Bertsch. Time-dependent local-density approximation in real time. *Phys. Rev. B*, 54:4484–4487, Aug 1996.
  - [32] T. Otobe, M. Yamagiwa, J. I. Iwata, K. Yabana, T. Nakatsukasa, and G. F. Bertsch. First-principles electron dynamics simulation for optical breakdown of di-

- electrics under an intense laser field. *PHYSICAL REVIEW B*, 77(16), APR 2008.
- [33] Yasushi Shinohara, Kazuhiro Yabana, Yosuke Kawashita, J-I Iwata, Tomohito Otobe, and George F Bertsch. Coherent phonon generation in time-dependent density functional theory. *Physical Review B*, 82(15):155110, 2010.
- [34] Kazuhiro Yabana, T Sugiyama, Y Shinohara, T Otobe, and GF Bertsch. Time-dependent density functional theory for strong electromagnetic fields in crystalline solids. *Physical Review B*, 85(4):045134, 2012.
- [35] Basile F. E. Curchod, Ursula Rothlisberger, and Ivano Tavernelli. Trajectory-Based Nonadiabatic Dynamics with Time-Dependent Density Functional Theory. *Chem. Phys. Chem.*, 14:1314, 2013.
- [36] George F Bertsch, J-I Iwata, Angel Rubio, and Kazuhiro Yabana. Real-space, real-time method for the dielectric function. *Physical Review B*, 62(12):7998, 2000.
- [37] Norman Troullier and José Luís Martins. Efficient pseudopotentials for plane-wave calculations. *Physical review B*, 43(3):1993, 1991.
- [38] M. Noda, S. A. Sato, Y. Hirokawa, M. Uemoto, T. Takeuchi, S. Yamada, A. Yamada, Y. Shinohara, M. Yamaguchi, K. Iida, I. Floss, T. Otobe, K.-M. Lee, K. Ishimura, T. Boku, G. F. Bertsch, K. Nobusada, and K. Yabanad. Salmon: Scalable ab-initio light-matter simulator for optics and nanoscience. *Comp. Phys. Comm.*, *in press*.
- [39] Web site of SALMON. <http://salmon-tddft.jp/>.
- [40] Yuta Hirokawa, Taisuke Boku, Shunsuke A Sato, and Kazuhiro Yabana. Electron dynamics simulation with time-dependent density functional theory on large scale symmetric mode xenon phi cluster. In *Parallel and Distributed Processing Symposium Workshops, 2016 IEEE International*, pages 1202–1211. IEEE, 2016.
- [41] J. P. Perdew and Alex Zunger. Self-interaction correction to density-functional approximations for many-electron systems. *Phys. Rev. B*, 23:5048–5079, May 1981.
- [42] Z X Hu, J Hedley, B J Gallacher, and I Arce-Garcia. Dynamic characterization of mems using raman spectroscopy. *J. Micromech. Microeng.*, 18:095019, 2008.
- [43] Yong]Xin Yan, Edward B. Gamble Jr., and Keith A. Nelson. Impulsive stimulated scattering: General importance in femtosecond laser pulse interactions with matter, and spectroscopic applications. *J. Chem. Phys.*, 83:5391–5399, 1985.